Photochemical & Photobiological Sciences (2022) 21:1387–1398
https://doi.org/10.1007/s43630-022-00229-9

ORIGINAL PAPERS

Influence of photosensitizer concentration and polymer composition on photoinduced antimicrobial activity of PVA- and PVA-chitosan-based electrospun nanomaterials cross-linked with tailor-made silicon(IV) phthalocyanine

Anzhela Galstyan[1,2] · **Konstantin Strokov**[2]

Received: 3 January 2022 / Accepted: 4 April 2022 / Published online: 5 May 2022

Abstract

The ongoing effort to eradicate pathogenic bacteria and viruses is a major endeavor that requires development of new and innovative materials. Materials based on photodynamic action represent an emerging and attractive area of research, and therefore, a broad understanding of chemical design principles is required. In the present study, we investigated the antibacterial and antiviral activities of five different nanofibrous membranes composed of poly(vinyl alcohol) or poly(vinyl alcohol)-chitosan mixture cross-linked through silicon(IV)phthalocyanine derivative with the aim to identify the role of the carrier polymer and photosensitizers concentration on its efficacy. A straightforward cross-linking process was adopted to create a water-stable material with an almost uniform distribution of the fiber structure, as revealed by scanning electron microscopy. The results of the antimicrobial studies showed that the increase in the amount of chitosan in the polymer mixture, rather than the increase in the photosensitizer concentration, enhanced the activity of the material. Due to their visible light-triggered antimicrobial activity, the resulting materials provide valuable opportunities for both topical antimicrobial photodynamic therapy and the area of environmental remediation.

Graphical abstract

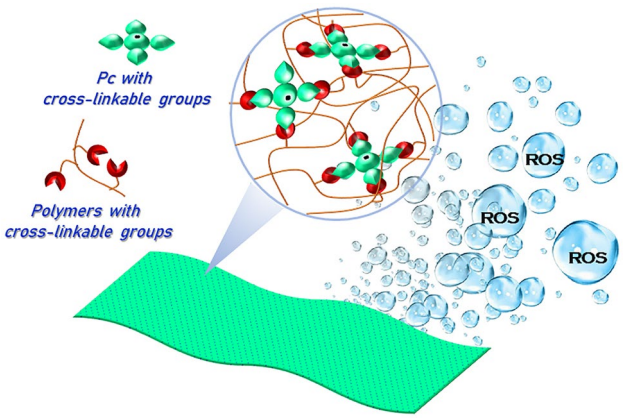

Keywords Phthalocyanine · Electrospinning · Photodynamic inactivation · Reactive oxygen species · Bacteria · Virus

✉ Anzhela Galstyan
anzhela.galstyan@uni-due.de

Extended author information available on the last page of the article

1 Introduction

The rise of antibiotic-resistant bacteria has called for the development of alternative antibacterial therapeutics [1]. In fact, most antibiotics have only one specific target, and therefore, it is only a matter of time until pathogens develop resistance to common antimicrobial agents [2]. In this regard, antimicrobial photodynamic therapy (aPDT) has gained increasing attention as a promising alternative for the treatment of resistant infections [3–5]. This method is based on the principle of activating photosensitizers (PS) by visible or near-infrared light to generate reactive oxygen species (ROS) that can attack and kill various microorganisms without causing resistance [6–8]. (Bio) materials bearing photoactive dyes expand the applications of aPDT and have great potential for improving the topical treatment of antibiotic-resistant and recurrent infections [9, 10]. Every day, resistant microorganisms are released into the environment, posing an increasing threat to public health. In this regard, materials capable of disinfecting water and eliminating pathogens responsible for water-borne diseases have a high potential for environmental remediation and are of particular interest [11, 12].

Combining aPDT with the outstanding potential of nanotechnology advanced, structurally controlled materials could be developed [13]. One of the best-known methods for nanofabrication is electrospinning [14, 15]. It is a versatile and promising technique for producing ultrafine nanoscale fibers generated by applying a high voltage to the tip of the polymer solution or melt. Nanofiber scaffolds have high porosity (above 80%), which provides high permeability, and submicron pore size, making them suitable for applications in different fields, such as microfiltration, tissue engineering, nanocatalysis, sensors, etc. Moreover, the ease of integrating special functions makes them an excellent candidate for the development of novel and efficient materials that can combine multiple properties in a single unit. For instance, Zhang et al. used nanocomposite fibers for one-step treatment of infections, where photodynamic sterilization of superbacteria and subsequent collagen regeneration reduced wound healing time from 24 to 16 days [16]. For the treatment of bacteria-infected wounds, recently, electrospun membrane consisting of two layers was reported [17]. While the first layer composed of poly(lactic-*co*-glycolic) acid and black phosphorus-grafted chitosan showed high antibacterial efficacy, the second layer composed of gelatin and ginsenoside could facilitate the migration and tube formation of human umbilical vein endothelial cells. In another study nanofiber materials containing ClIn(III) octacarboxy phthalocyanine alone or conjugated to magnetic nanoparticles were successfully used in aPDT and for photodegradation of methyl red [18].

Poly(vinyl alcohol) (PVA) is one of the most widely used polymers for the production of electrospun materials that are employed in various biomedical applications, ultrafine filters, or protective clothing [19]. PVA-based materials are non-toxic, biodegradable, have excellent mechanical properties and good flexibility [20, 21]. However, many hydroxyl groups of the PVA polymer make it very soluble in water, thus, an additional step, such as cross-linking with glutaric acid, is required in their production to obtain water-resistant materials [22, 23]. Recently, we reported the one-pot fabrication of electrospun nanomaterials based on PVA and polyethylene glycol functionalized silicon(IV) phthalocyanine where both components were thermally cross-linked by esterification using sebacic acid as a cross-linking agent [24]. The fabricated nanomaterials were found to reduce the viability of Gram-positive bacteria upon irradiation while having low cytotoxic effects on human fibroblasts and being effective against bacterial fouling.

Despite the good processability of petro-based polymers in recent years, the utilization of biomaterials obtained from renewable raw sources (e.g. chitin/chitosan, starch, cellulose, lignin, etc.) has experienced rapid growth [25, 26]. The animal or plant origin of the polymers is not only an environmentally friendly alternative to synthetic polymers but also offers highly advantageous material properties, especially high biocompatibility, biodegradability, and in some cases, antimicrobial properties. Yet, these materials also present many inherent challenges, such as low spinnability potential and the need for post-cross-linking treatment to achieve the desired water resistance. Chitosan (CS) is widely used biomaterial, which is gaining increasing interest due to its inherent antibacterial activity [27]. It could be obtained from chitin, which can be extracted from shellfish like shrimp, lobster, and crab. Since it is a natural macromolecule, the materials made from it are considered sustainable and environmentally friendly [28]. The poor mechanical properties of CS could be improved using a synthetic biodegradable polymer such as PVA as a supplement. Hybrid nanomaterials based on PVA and CS have a very important feature: hydrogen bonds between two polymers stabilize their structure. These types of composite materials, particularly in the form of nanostructures, have novel functionalities and are widely used for certain biomedical applications, as well as for the removal of hazardous pollutants such as carbon monoxide from the air [29] or selected toxic ions such as Pb(II) and Cd(II) from wastewaters [30]. In recent years, PVA-CS composite nanofibers exhibiting antibacterial activity upon addition of various antibacterial reagents have been developed. Using a mixture of PVA-CS 7:3 and Cu-based MOF composite fibers for wound dressing material has been recently reported [31]. In another study, nanofibrous PVA-CS was used as a dual drug delivery system for

lidocaine hydrochloride and erythromycin-loaded gelatin nanoparticles as an antibiotic [32]. The authors showed that the best bead-free morphology for nanofiber materials was obtained when the weight ratio of PVA to CS solution was 96:4. PVA-CS composite nanofibers were also used for the delivery of photosensitizers such as indocyanine green. The nanofibrous material, obtained from an optimized electrospinning solution consisting of 7% (w/v) PVA and 2% (w/v) CS, showed obvious inhibition effects on antibiotic-resistant bacteria [33]. In that study, the antimicrobial effect was due to the released PS, which was initially delivered to the media very rapidly and then steadily. In the systems where PS is covalently bound, the antimicrobial effect depends on the close contact between the material and the microorganism. Recently, we investigated the antimicrobial properties of nanofiber materials based on different types of polymers containing entrapped or covalently bound PS and showed that the molecular and physical properties of the carrier polymers play a more important role in the overall activity of the materials than the concentration and binding mode of PS. However, further studies are needed to better understand the interplay between the composition of the material and the effectiveness of photo-triggered inactivation.

In this study, we used only PVA or PVA-CS mixture together with water-soluble silicon(IV) phthalocyanine-based PS with four carboxyl groups to prepare electrospun nanofibers in which all components were linked by PS without the need for an additional cross-linker. The antimicrobial activity against Gram-positive *B. subtilis* and Gram-negative *E. coli* bacteria and bacteriophages MS2 and phi6 as model organisms were investigated to find out whether an increase in PS or CS load affects the activity of the material to a greater extent. Several important properties of the obtained electrospun fiber membranes were characterized (Fig. 1).

2 Materials and methods

2.1 General

All solvents, chemicals, buffer salts, and nutrient broths were purchased from Fisher Scientific, TCI, Sigma-Aldrich, Acros Organics, or Alfa Aesar and used as received. Ultrapure deionized water used for all media and buffers was provided by Thermo Scientific Barnstead GenPure UV/UF Systems. Steady-state absorption and emission spectra were recorded in an Infinite 200 Pro M Plex multi-mode microplate reader (Tecan Group Ltd., Zürich, Switzerland). $SiPc(COOH)_4$ was synthesized using previously published methods [7, 34].

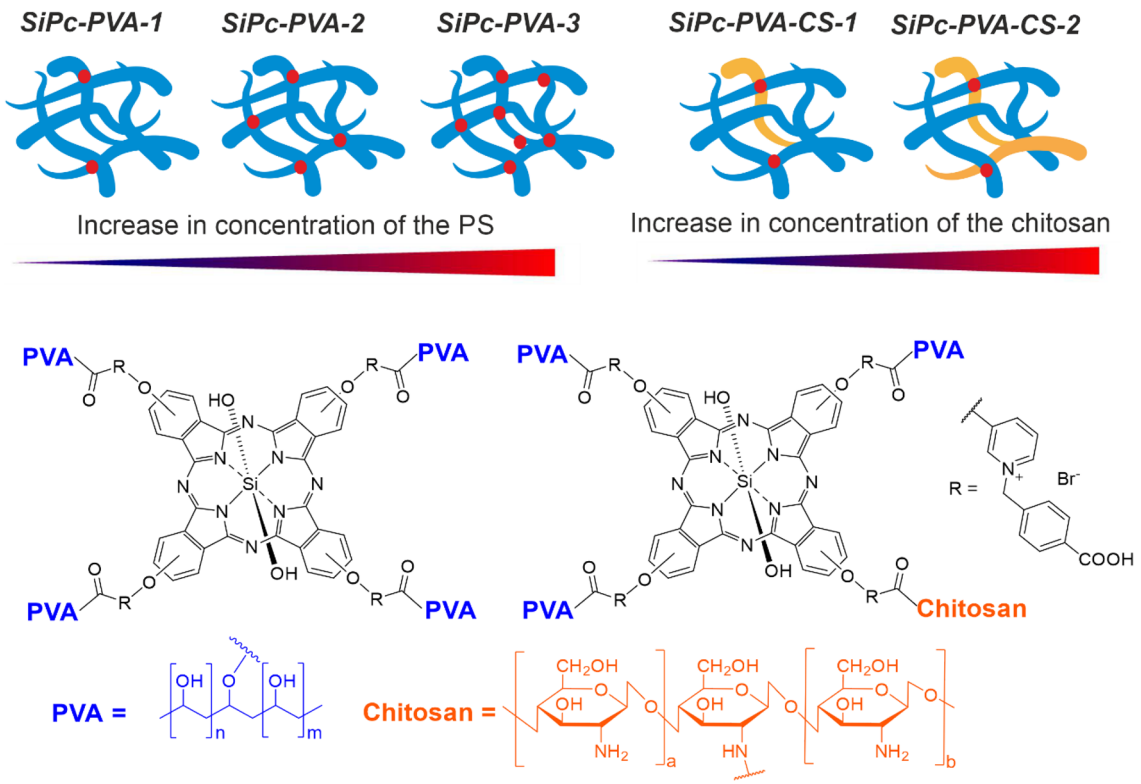

Fig. 1 Schematic representation of the composition of the nanofiber materials used in this study

2.2 Electrospinning

Membranes were electrospun using two 5 mL syringes with metal needles 20G, a distance of 15 cm, and a rotation speed of the collector 500 rpm. For PVA-based NFs, PVA solution (10 w% MW = 146–186 kDa, 98.0–99.8% degree of hydrolysis) was prepared by dissolving PVA in H_2O and stirring at 90 °C overnight. After cooling to RT the corresponding amount of $SiPc(COOH)_4$ (18, 36, or 72 mg predissolved in 1 mL DMF) was added to 19 mL PVA solution. The obtained mixture was stirred at rt for 3 h, cooled, and then electrospun (15 kV, flow rate 1.2 mL/min). After electrospinning NFs were heated at 120 °C for 1 h. For PVA-CS nanofibers first PVA and chitosan mixtures were prepared in a 9:1 or 4:1 ratio. Subsequently, $SiPc(COOH)_4$ (18 mg, pre-dissolved in 1 mL DMF) was added to the 19 mL PVA-CS mixture, which was stirred at rt for 3 h and electrospun (20 kV for SiPc-PVA-CS-1 and 25 kV for SiPc-PVA-CS-2, flow rate 0.6 mL/min). Electrospinning was done using electrospinner NFES-100 (Micro&Nano Tools, Niagara Falls, Canada). FT-IR spectra were measured on a Bruker IFS 55 Fourier transform infrared spectrometer (Bruker Corporation, Billerica, Massachusetts, USA).

2.3 Scanning electron microscopy measurements

SEM images were taken by HITACHI SU8230 scanning electron microscope (Hitachi Ltd. Corporation, Tokyo, Japan). To perform SEM measurements, the samples were sputter-coated with Ag and imaged with an accelerating voltage using Zeiss SmartSEM software. Image j (NIH) (Bethesda, MD) was used to determine the diameter of the fibers in the NFs.

2.4 Contact angle measurements

The degree of wettability of NFs was assessed and compared through measurement of the contact angle by allowing a single drop of distilled water to stand and spread on the surface for the 30 s. A pendant drop tensiometer DSA100 (Krüss, Hamburg, Germany) was used.

2.5 In vitro swelling study

Water absorption capacities of the prepared scaffolds were determined by immersing a square piece (12 mm diameter) of NF in water at room temperature. Once the equilibrium was reached (~ 1 h), the samples were removed and the surface wetness was removed using filter paper. The following equation is used to calculate the equilibrium-swelling ratio.

$$\text{Swellin}\ (\%) = W_i - W_f / W_i \times 100,$$

where W_i and W_f are the initial and final weight of the scaffold, respectively.

2.6 Determination of photosensitizers concentration in materials

UV–Vis spectroscopy was used to determine the PS loading. To obtain a constant area of approximately 113 mm^2, samples were randomly cut from the mat at different locations using a 12 mm diameter hole punch. The samples were washed with 70% ethanol solution (1 × 1 mL) and water (3 × 1 mL) to remove unbound PS and then heated at 100 °C for 1 h in a 1 mL DMF-H_2O 1:1 mixture.

2.7 Bacterial strains and culture conditions

Bacillus subtilis strain DB104 and *E. coli* strain Nissle 1917 were grown on lysogeny broth (LB) agar and kept at 4 °C. A single isolated colony was picked from this plate, transferred to 3 mL LB broth, and incubated aerobically overnight at 37 °C in a shaker incubator at 180 rpm (rotations per minute). The following day, bacteria were suspended in 10 mL of fresh LB medium to an optical density OD600 = 0.1 and grown in a flask to attenuation of approximately OD600 = 0.4. Thereafter, the bacterial suspensions were centrifuged at 4000 rpm for 5 min, resuspended in a buffer solution to the final bacterial concentration of approximately 1×10^{-7} cells per mL, and used for the experiments.

2.8 Photoinactivation of bacteria

Before irradiation experiments, nanomaterials were treated with 70% aqueous ethanol solution for 1 h and then washed with a sufficient amount of PBS to disinfect them and remove unbound PSs. Each Ø12 mm membrane was incubated with approximately 200 µL bacterial suspension for 15 min and irradiated with an LED lamp (660 ± 24 nm) for a certain duration. A power meter (Solar Meter from Solartech) was used to measure fluence rates regularly. After irradiation, viable bacterial cells were determined by serial dilutions of the bacterial suspension plated on Luria–Bertani agar plates. The number of CFU/mL was calculated using a ProtoCOL automatic colony counter from Synbiosis.

2.9 Quantification of bacteria adherent on membranes

Ø12 mm pre-sterilized and washed membranes were immersed in the 200 µL bacterial suspension (ca. 1×10^{-8} cells per mL) in a 24-well plate under static conditions at 37 °C for 1 h and were washed carefully with PBS afterwards. The XTT assay which is based on the reduction of 2,3-bis-(2-methoxy-4-nitro-5-sulfophenyl)-5-[(phenylamino)carbonyl]-2H-tetrazolium hydroxide (XTT) in the metabolically active microbial cells to a water-soluble formazan was used to determine the viable cells attached to the nanomaterial. 200 µL of XTT-menadione solution was prepared as described previously [7] and added to electrospun membranes. After incubation for 7 h an aliquot of 100 µL was then taken, transferred to a 96-well plate and absorbance was recorded at 492 nm with a microplate reader (Tecan, Switzerland). The results are expressed as the relative viability (% control).

2.9.1 Virus strains and methods.

Stocks of bacteriophages phi6 DSM 21518 and MS2 DSM 13767 and the corresponding host cells Pseudomonas syringae van Hall 1902 DSM-21482 and Escherichia coli DSM-5695 were purchased from DSMZ Germany. The stocks were each rehydrated in 500 µL of sterile PBS. Propagation was carried out according to the specifications provided by the Leibniz Institute DSMZ–German Collection of Microorganisms and Cell Cultures GmbH (Braunschweig, Germany). 50 mL of exponential phase growth culture of Pseudomonas syringae van Hall or *E. coli* host cell LB broth was infected with 50 µL of phi6 or MS2, correspondingly, and incubated at 25 °C (phi6) or 37 °C (MS2) with gentle shaking at 80 rpm for 48 h until *E. coli* cells were completely lysed. The lysate was then filtered using 0.22 µm pore size filter unit (Millipore) to remove the bacterial cell debris. The infectivity and titer of the filtrate was then determined to know the concentration of the virus. Photodynamic inactivation of bacteriophages phi6 and MS2 was investigated using prewashed and sterilized nanofiber membranes. Double-layer agar plaque assays were carried out before and after irradiation to determine the extension of phage inactivation.

2.10 Statistical analysis

Data are expressed as mean ± standard deviation. Student's *t* test and one-way analysis of variance within groups were used to compare the treatment effects. $p < 0.05$ was considered to represent a significant difference.

3 Results and discussion

3.1 Fabrication and morphology of materials

The PVA and PVA-CS mats containing $SiPc(COOH)_4$ as photosensitizers were prepared by a well-established electrospinning technique. Based on data from previous work [24], an optimum concentration for PVA suitable for electrospinning was determined to be 10% (w/v). Different amounts of PS (0.9, 1.8, or 3.6 mg/mL) were suspended in the PVA solution, electrospun, and subsequently cross-linked by heating the membranes at 120 °C for 1 h. PVA-CS nanocomposite fibers were prepared in the same way from the solution containing different ratios of polymers but the same amount of $SiPc(COOH)_4$ (0.9 mg/mL PVA-CS solution). In SiPc-PVA-CS-1, weight ratio of PVA and Chitosan was fixed to 9:1 and in SiPc-PVA-CS-2 at 4:1. Since changing the solution composition changes the viscosity and conductivity, the electrospinning parameters were optimized with each mixture to obtain bead-free mats. While a voltage of 15 kV was sufficient for the successful formation of PVA-based mats, the addition of CS under the same conditions resulted in discontinuous fibers and the appearance of beads, due to the increase of repulsive forces between the ionic groups of the polymers. This could be remedied by increasing the voltage to 20 kV for SiPc-PVA-CS-1 or 25 kV for SiPc-PVA-CS-2.

The morphology of the cross-linked nanofiber films was analyzed with SEM and is presented in Fig. 2 and Fig. S1 in the Supporting Information. In all cases, a network of continuous, relatively homogenous nanosized fibers was formed, but the diameters of the fibers were different. The rising concentration of $SiPc(COOH)_4$ lead to the gradual increase of the nanofiber diameter in the PVA-based mats. The average diameter of SiPc-PVA-1, SiPc-PVA-2, and SiPc-PVA-3 mats increased correspondingly from about 396 ± 146 nm to 479 ± 181 nm to 608 ± 180 nm. The reason for the larger fiber diameters is most likely the higher viscosity of the solution [35, 36]. Increasing the voltage and the ratio between chitosan and PVA in the solution leads to a decrease in the average fiber diameter from 546 ± 207 nm for SiPc-PVA-CS-1 to 373 ± 146 nm for SiPc-PVA-CS-2. For PVA-CS-2 without

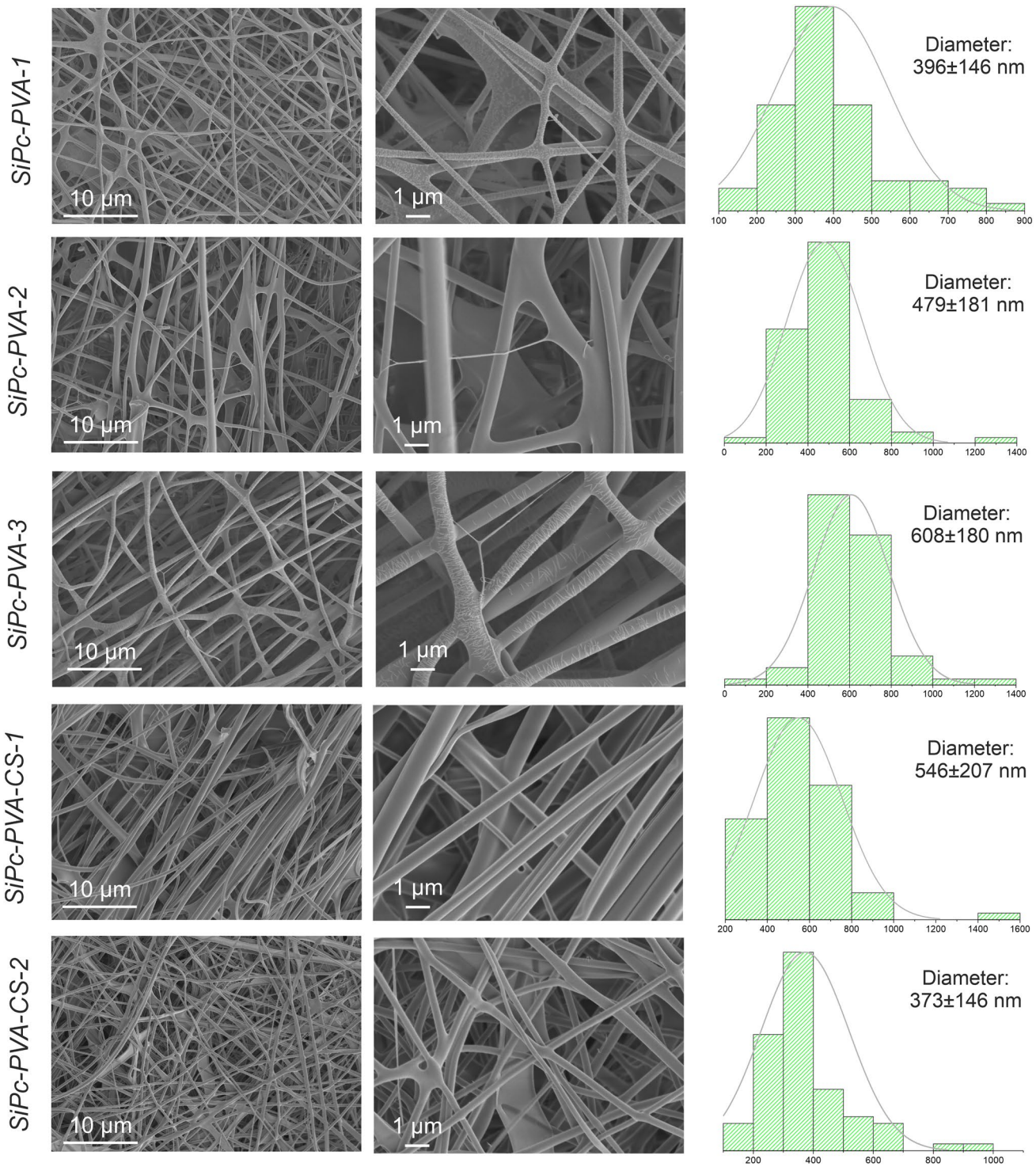

Fig. 2 SEM images and fiber diameter distribution of nanofiber materials

photosensitizer, which was prepared for control experiments, the fiber diameter of about 459 ± 179 nm is only slightly different from that of SiPc-PVA-CS-2. This is in agreement with the results of Karimi et al. whose studies revealed that the thickness of the fibers increases with an increase in the applied voltage and with a decrease in the chitosan/PVA ratio [37].

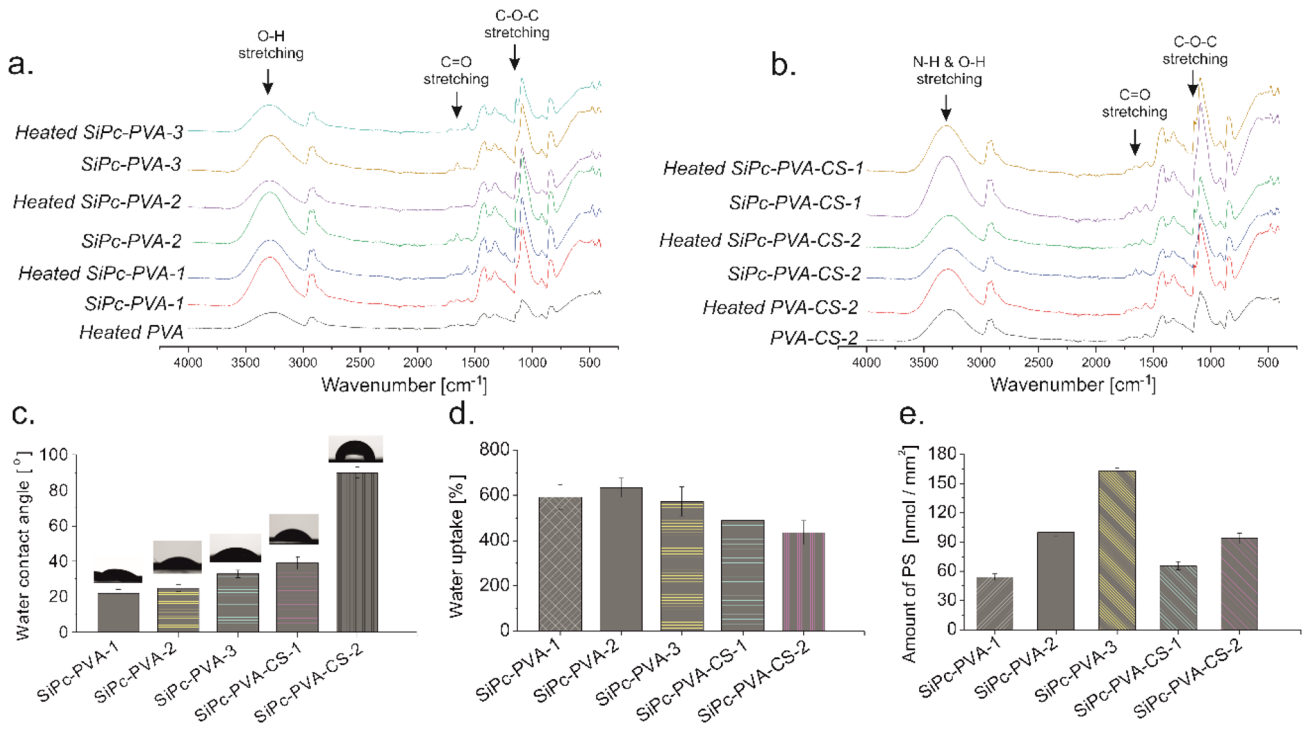

Fig. 3 Characterization of nanofiber materials; **a** FT-IR spectra of PVA-based materials, **b** FT-IR spectra of PVA-CS-based materials, **c** water contact angle, **d** water uptake ability, and **e** amount of PS in membranes determined using UV–Vis spectroscopy

3.2 Characterization of materials

Measurement by FT-IR was performed to characterize the functional groups involved in the formation of the nanocomposite fibers. Figure 3a and 3b show FT-IR spectra of PVA and PVA-CS-based nanofibers before and after thermal cross-linking. All spectra display characteristic broadband of OH and NH_2 groups in the range of 3700–3000 cm^{-1}, which decreases when the mats undergo thermal treatment. Moreover, in the spectra of the heated films, the band at 1653 cm^{-1} ascribed to the C=O valence vibration of the carboxylic acids almost completely disappeared, while the peak at 1141 cm^{-1} corresponding to the C–O stretching vibration increased, suggesting that cross-linking of the $SiPc(COOH)_4$ and PVA or PVA-CS occurred upon heating. In contrast, the peak at 1656 cm^{-1} in PVA-CS-2 showed no considerable difference before and after thermal treatment.

The wettability and water absorption capacity are considered to be important properties of interfaces that are supposed to be used in aqueous media and are commonly determined by both the chemical composition and the overall geometric microstructure of the interfaces. The contact angles of the cross-linked nanofiber mats were measured to investigate their interaction with aqueous media. By varying the $SiPc(COOH)_4$ amount, the hydrophilicity of PVA-based mats was not affected too much; an increase from 22° ± 2° to 33° ± 2° degree was observed. The addition of CS was found to influence the surface wettability to a higher extend. As shown in Fig. 3c, the water contact angle of SiPc-PVA-CS-1 after thermal treatment is about 40°, while increasing the CS ratio resulted in a much higher value for SiPc-PVA-CS-2, which is about 90°. The change in wetting dynamics could be associated with the relatively hydrophobic chitosan backbone, but the small fiber diameter and small voids of SiPc-PVA-CS-2 also have a critical impact on the water contact angle. This is consistent with previous studies showing that the water contact angle of the electrospun chitosan membrane was above 120° [38, 39].

Nevertheless, the presence of hydrophilic groups such as OH, NH_2, and COOH in both PVA and CS endow the nanofiber membranes with a high swelling degree in water. Figure 3d shows water uptake of the membranes after 1 h incubation in aqueous media. PVA-based membranes showed identical water uptake, ranging from 573 to 634% while increasing chitosan concentration in the electrospinning solution led to a slight decrease in the values. Therefore, the SiPc-PVA-CS-1 could absorb 489% and SiPc-PVA-CS-2 435% water. Not only composition but also other factors, such as the porosity of the scaffold, affect the water absorption capability of the membranes; higher porosity increases the ability of the material to absorb a greater amount of water.

UV spectroscopy was used to determine the amount of PS in the nanofiber mats after washing to remove unbound

PS (1 × 70% ethanol solution and 3 × water). The materials were dissolved in *N,N*-dimethylformamide: water 1:1 mixture when heated at 100 °C for 1 h, and the amount of PS was calculated from the calibration curve of $SiPc(COOH)_4$ obtained in the same solvent mixture (Fig. S3, Supporting Information). As expected, the PS content increases in the SiPc-PVA1 to SiPc-PVA-3 series. Despite the same initial concentration, the amount of PS was found to be higher in the CS-containing materials, which is probably due to the additional cross-linking and other non-covalent interactions of PS with CS (Fig. 3e).

3.3 Antibacterial performance of the membranes

The antibacterial activity of the membranes was evaluated against two typical generic bacteria Gram-positive *B.°subtilis* strain DB 104 and Gram-negative *E.°coli* strain Nissle 1917. Studies were performed by counting the number of colony-forming units (CFUs) on LB plates seeded with the bacterial suspension after being irradiated for a specified time in the presence of the corresponding membrane. The control groups (nanomaterials containing PS in the dark or nanomaterials without PS) showed no bacterial inactivation under the same conditions—light dose or time, indicating that neither NIR light nor the PS in the absence of illumination is lethal to bacteria. This is consistent with previously published studies in which CS was used in combination with various PS in photodynamic inactivation studies [40–42]. Although chitosan itself is known to possess antimicrobial properties and can be used in agricultural, food, and biomedical applications [43], its intrinsic antibacterial activity is not suitable for applications requiring rapid and drastic reduction of microbial populations. The mode of action of CS is mainly related to its ability to bind to cell membrane components, chelate ions or nutrients, and affect the synthesis of DNA/RNA or proteins when taken up by cells.

As shown in Fig. 4, independent of the content of PS, all PVA-based membranes did not exhibit any antibacterial activity. However, there was a noticeable increase in antimicrobial activity of CS-containing samples against both Gram-positive and Gram-negative strains when irradiated with light doses of 63 J/cm^2. As could be seen from Fig. 4a the viability of *B.°subtilis* DB104 was reduced by 95.64%, 1.36 $\log_{10,}$ and 99.90%, 2.98 $\log_{10}$ in the presence of SiPc-PVA-CS-1 and SiPc-PVA-CS-2, respectively. aPDT activity against *E. coli* Nissle 1917 was comparable; 96.02%, 1.40 $\log_{10}$ reduction was observed in the case of SiPc-PVA-CS-1 and 98.56%, 1.84 $\log_{10}$ for SiPc-PVA-CS-2 (Fig. 4b). The similarity in inactivation efficacy is somewhat unexpected, as the difficulties in killing Gram-negative bacteria are well known and have been studied in detail [44]. Indeed, in our recent study,

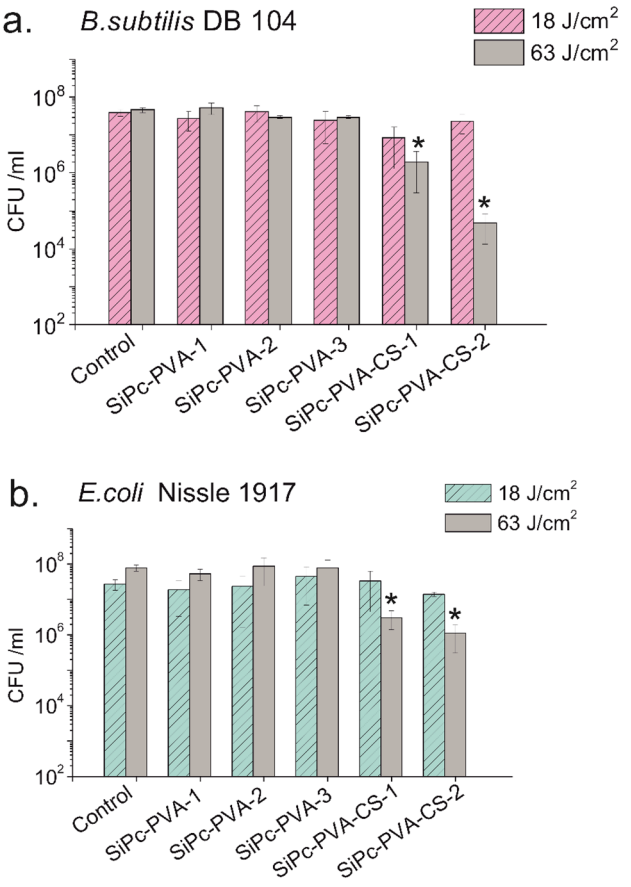

Fig. 4 Antibacterial photodynamic inactivation efficacy of PVA and PVA-CS electrospun materials for **a** Gram-positive *B.°subtilis* DB104 and **b** Gram-negative *E.°coli* Nissle 1917. Error bars correspond to the standard deviation ($n = 3$)

we showed that PVA-based electrospun nanomaterials cross-linked via axially functionalized silicon(IV)phthalocyanine derivative was very efficient in inactivation of Gram-positive *S. aureus* 3150/12, *S. warneri* 3930/16, and *B. subtilis* DB104 [24]. In another study, we have used zinc(II)phthalocyanine derivatives as PS and three different polymers, PVA, polyacrylonitrile (PAN), and poly(δ-caprolactone) (PCL), for the fabrication of nanomaterials. Although among the three different polymers, PAN- and PCL-based scaffolds exhibited the highest antimicrobial activity due to dominant dipole–dipole or hydrophobic interactions, PVA-based scaffolds were also able to achieve > 5$\log_{10}$ reduction of Gram-positive *B.°subtilis* upon prolonged irradiation [45]. In their recent study, group of Ghiladi have used UV-photocrosslinkable polymer *N*-methyl-4(4′-formyl-styryl)pyridinium methosulfate acetal poly(vinyl alcohol) and different PSs to coat commercially available materials. Upon illumination, the coated materials were able to inactivate Gram-positive *S.°aureus* ATCC-29213 by 97–99.999% [46]. In general,

two main factors can contribute massively to the aPDT activity of PVA-based membranes: (1) a tightly bound hydration layer can prevent a close interaction between microorganisms and nanomaterial, and (2) diffusion of oxygen into the material and subsequent diffusion range of the generated ROS. The considerable increase in activity for PVA-CS composites despite the lower amount of PS could be due to the stronger interaction between bacteria and material surface due to the additional surface functionality and increased hydrophobicity as evidenced by contact angle measurements. Recent research has shown that both superhydrophobic and superhydrophilic surfaces can inhibit the close association of bacteria with a surface on which ROS can reach cells, so only materials that are neither too hydrophilic nor too hydrophobic can be efficient in photodynamic inactivation [47]. To show the differences in the interactions between the nanomaterial and the bacteria, we estimated amount of adherent bacteria after 1 h of incubation using the XTT assay. Although the results showed that the amount of metabolically active bacteria was higher on CS-containing materials, as expected (Fig. S5, Supporting Information), the differences did not correlate well with the differences in contact angle. This could be due to the long (7 h) incubation of the bacteria-bound membranes with 2,3-bis-(2-methoxy-4-nitro-5-sulfophenyl)-5-[(phenylamino)carbonyl]-2H-tetrazolium hydroxide (XTT) to convert it to a water-soluble formazan, in which the intrinsic antimicrobial activity of CS may play a role.

Gas mobility in the nanomaterial also plays a key role in assessing the activity of the material, since the access of the oxygen molecule to the excited photosensitizer is required for ROS generation and, on the other hand, the generated ROS should diffuse to react to its target. The type of polymer can play a significant role in this regard. For example, to demonstrate the differences in O_2 permeability in the different polymer matrices, Mosinger et al. performed time-resolved single-point phosphorescence measurements at 1270 nm using a polystyrene and gelatin nanofiber materials containing a tetraphenylporphyrin as PS [48]. Gelatin nanofiber material produced significantly less $^1O_2$ in this case, which was attributed the lower oxygen permeability of gelatin. Considering that among the different types of ROS, $OH^{\cdot}$ has the shortest diffusion range and the bacterial membrane permeability of $O_2^{\cdot -}$ is rather low, one could assume that $^1O_2$ with a diffusion range of ca. 200 nm is most likely the preferred ROS for photoactive nanomaterials [49, 50]. Using 9,10-anthracenediyl-bis(methylene)dimalonic acid as a chemical trap for $^1O_2$ and 2′,7′-dichlorofluorescein diacetate as a general ROS probe, we showed in our previous study that $SiPc(COOH)_4$ does not generate $^1O_2$ but rather generates other types of ROS [24, 34]. The complete lack of activity of PVA-based materials against bacteria is most likely due to the inability of $SiPc(COOH)_4$ to generate $^1O_2$. This is also feasible considering the highly aggregated state of PS, as evident from the UV–Vis reflectance spectra (Fig. S2, Supporting Information).

3.4 Antiviral performance of the membranes

Although viruses cannot replicate independently without a host cell, they can survive on surfaces for a long time [51]. Among various strategies used to decontaminate interfaces, the development of broadly applicable self-cleaning materials is highly desirable. Visible light-responsive triplet photosensitizer nanofiber membranes are particularly well suited for virus inactivation due to their rapid action and lack of resistance induction and could be used in personal protective equipment, air filters, and membrane-based water filters [52, 53]. Because bacteriophages are known to respond to photodynamic action in a manner similar to mammalian viruses [54], antiviral photodynamic inactivation studies were performed using bacteriophages MS2 as a model system for human non-enveloped RNA viruses and phi6 as a surrogate for enveloped RNA viruses. In contrast to the antibacterial results, both PVA- and PVA-CS-based materials were able to induce complete photodynamic inactivation of MS2 and phi6 upon irradiation with 63 J/cm^2 light doses. Under low light irradiation (18 J/cm^2), PVA-based membranes were able to induce approximately 1.5 $\log_{10}$ titer reduction of MS2. The activity of PVA-CS-based materials was 3–4-fold higher. In the case of phi6, only SiPc-PVA-CS-2 showed 99.67%, 2.48 $\log_{10}$ PFU (plaque-forming units) reduction when irradiated with the 18 J/cm^2 light doses. These results were somewhat unexpected since the viral envelope is considered the main target of ROS and enveloped viruses are usually more susceptible to photodynamic inactivation due to the easy destruction of the phospholipid bilayer [55]. Nevertheless, studies on the targets of antiviral PDI have shown that the viral genome could be an equally valid target for photoinactivation [56]. Yet, it is challenging to pinpoint the specific viral target responsible for lethality, and it is certainly feasible that a combination of damages takes place. It should be considered that the activity of the membranes depends not only on the ROS-induced damage but also on electrostatic and hydrophobic interactions occurring on the surfaces of the materials, which can cause morphological and conformational changes that affect the overall activity of the material (Fig. 5).

4 Conclusions

Killing microorganisms by visible light using photodynamic action is one of the most promising strategies for rapid and effective decontamination. The range of applications could be expanded by developing nanoscale materials with

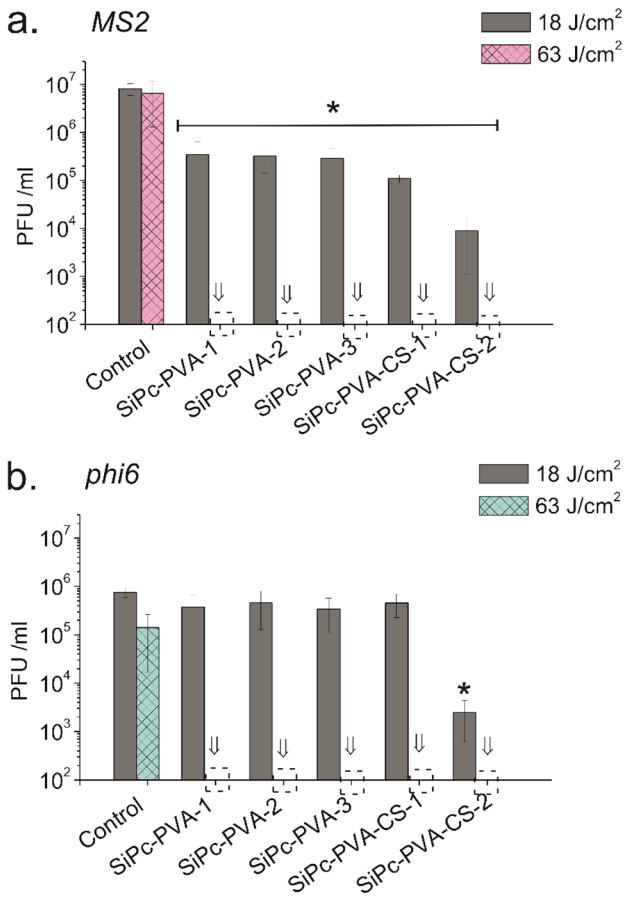

Fig. 5 Antiviral photodynamic inactivation efficacy of PVA and PVA-CS electrospun materials for bacteriophages **a** MS2 and **b** phi6. Error bars correspond to the standard deviation ($n = 3$)

effective photodynamic efficacy. In this study, we successfully used PVA or a PVA-CS mixture and four-armed water-soluble silicon(IV) phthalocyanine derivative to prepare water-stable red light-sensitive antibacterial and antiviral nanofibers. Silicon(IV) phthalocyanine served not only as a triplet photosensitizer but also as a cross-linking agent, due to the presence of four carboxyl groups at the periphery of the macrocycle. Our results showed that the addition of CS is crucial for the inactivation of sufficient numbers of bacteria, but it is clear that the type of generated ROS and gas mobility also play an important role. Inactivation of bacteriophages used as surrogates for mammalian viruses was more efficient, possibly due to the generation of ROS in the vicinity of the microorganism that correlates with a mechanism of action involving short-lived radicals. Due to the simplicity of modulating their activity, low cost of the components and high biocidal efficacy, these electrospun nanomaterials can find application in medicine and water treatment systems. The strategic expansion of this family of materials will promote the development of intelligent next-generation self-disinfecting and environmentally friendly systems. Detailed biological studies need to be conducted to understand why certain microorganisms are more sensitive than others.

Supplementary Information The online version contains supplementary material available at https://doi.org/10.1007/s43630-022-00229-9.

Acknowledgements Financial support of by the University of Duisburg Essen, Deutsche Forschungsgemeinschaft DFG GA2362/2-1 and Fonds der Chemischen Industrie is greatly acknowledged. We thank Martin Bühner (NanoAnalytics GmbH, Münster) for the SEM measurements.

Funding Open Access funding enabled and organized by the Projekt DEAL.

Declarations

Conflict of interest On behalf of all authors, the corresponding authors state that there is no conflict of interest.

References

1. Aroso, R. T., Schaberle, F. A., Arnaut, L. G., et al. (2021). Photodynamic disinfection and its role in controlling infectious diseases. *Photochem Photobiol Sci*, *20*, 1497–1545.
2. Hwang, T. J., Gibbs, K. A., Podolsky, S. H., & Linder, J. A. (2015). Antimicrobial stewardship and public knowledge of antibiotics. *The Lancet Infectious Diseases, 15*, 1000–1001.
3. Wainwright, M., Maisch, T., Nonell, S., Plaetzer, K., Almeida, A., Tegos, G. P., & Hamblin, M. R. (2017). Photoantimicrobials—Are we afraid of the light? *The Lancet Infectious Diseases, 17*, e49–e55.
4. Aroso, R. T., Schaberle, F. A., Arnaut, L. G., & Pereira, M. M. (2021). Photodynamic disinfection and its role in controlling infectious diseases. *Photochemical and Photobiological Sciences, 20*, 1497–1545.
5. Galstyan, A. (2021). Turning photons into drugs: Phthalocyanine-based photosensitizers as efficient photoantimicrobials. *Chemistry A European Journal, 27*, 1903–1920.
6. Cieplik, F., Deng, D., Crielaard, W., Buchalla, W., Hellwig, E., Al-Ahmad, A., & Maisch, T. (2018). Antimicrobial photodynamic therapy—What we know and what we don't. *Critical Reviews in Microbiology, 44*, 571–589.
7. Galstyan, A., Schiller, R., & Dobrindt, U. (2017). Boronic acid functionalized photosensitizers: A strategy to target the surface of

bacteria and implement active agents in polymer coatings. *Angewandte Chemie International Edition, 56*, 10362–10366.
8. Galstyan, A., Putze, J., & Dobrindt, U. (2018). Gaining access to bacteria through (reversible) control of lipophilicity. *Chemistry A European Journal, 24*, 1178–1186.
9. Mesquita, M. Q., Dias, C. J., Neves, M. G. P. M. S., Almeida, A., & Faustino, M. A. F. (2018). Revisiting current photoactive materials for antimicrobial photodynamic therapy. *Molecules, 23*, 2424.
10. Zarrintaj, P., Moghaddam, A. S., Manouchehri, S., Atoufi, Z., Amiri, A., Amirkhani, M. A., Nilforoushzadeh, M. A., Saeb, M. R., Hamblin, M. R., & Mozafari, M. (2017). Can regenerative medicine and nanotechnology combine to heal wounds? The search for the ideal wound dressing. *Nanomedicine, 12*, 2403–2422.
11. Ballatore, M. B., Durantini, J., Gsponer, N. S., Suarez, M. B., Gervaldo, M., Otero, L., Spesia, M. B., Milanesio, M. E., & Durantini, E. N. (2015). Photodynamic inactivation of bacteria using novel electrogenerated porphyrin-fullerene C60 polymeric films. *Environmental Science and Technology, 49*, 7456–7463.
12. Majiya, H., Chowdhury, K. F., Stonehouse, N. J., & Millner, P. (2019). TMPyP functionalised chitosan membrane for efficient sunlight driven water disinfection. *Journal of Water Process Engineering., 30*, 100475.
13. Kaspar, C., Ravoo, B. J., van der Wiel, W. G., Wegner, S. V., & Pernice, W. H. P. (2021). The rise of intelligent matter. *Nature, 594*, 345–355.
14. Liao, Y., Loh, C.-H., Tian, M., Wang, R., & Fane, A. G. (2018). Progress in electrospun polymeric nanofibrous membranes for water treatment: Fabrication, modification and applications. *Progress in Polymer Science, 77*, 69–94.
15. Taskin, M. B., Ahmad, T., Wistlich, L., Meinel, L., Schmitz, M., Rossi, A., & Groll, J. (2021). Bioactive electrospun fibers: Fabrication strategies and a critical review of surface-sensitive characterization and quantification. *Chemical Reviews, 121*, 11194–11237.
16. Zhang, J., Liu, C.-L., Liu, J.-J., Bai, X.-H., Cao, Z.-K., Yang, J., Yu, M., Ramakrishna, S., & Long, Y.-Z. (2021). Eluting mode of photodynamic nanofibers without photosensitizer leakage for one-stop treatment of outdoor hemostasis and sterilizing superbacteria. *Nanoscale, 13*, 6105–6116.
17. Zhou, L., Liu, N., Feng, L., Zhao, M., Wu, P., Chai, Y., Liu, J., Zhu, P. & Guo, R. (2021). Multifunctional electrospun asymmetric wettable membrane containing black phosphorus/Rg1 for enhancing infected wound healing, *Bioengineering and Translational Medicine,* e10274.
18. Sindelo, A., & Nyokong, T. (2019). Magnetic nanoparticle—Indium phthalocyanine conjugate embedded in electrospun fiber for photodynamic antimicrobial chemotherapy and photodegradation of methyl red. *Heliyon, 5*, e02352.
19. Teodorescu, M., Bercea, M., & Morariu, S. (2019). Biomaterials of PVA and PVP in medical and pharmaceutical applications: Perspectives and challenges. *Biotechnology Advances, 37*, 109–131.
20. Chaouat, M., Le Visage, C., Baille, W. E., Escoubet, B., Chaubet, F., Mateescu, M. A., & Letourneur, D. (2008). A novel cross-linked poly(vinyl alcohol) (PVA) for vascular grafts. *Advanced Functional Materials, 18*, 2855–2861.
21. Chiellini, E., Corti, A., D'Antone, S., & Solaro, R. (2003). Biodegradation of poly(vinyl alcohol) based materials. *Progress in Polymer Science, 28*, 963–1014.
22. Truong, Y. B., Choi, J., Mardel, J., Gao, Y., Maisch, S., Musameh, M., & Kyratzis, I. L. (2017). Functional cross-linked electrospun polyvinyl alcohol membranes and their potential applications. *Macromolecular Materials and Engineering, 302*, 1700024.
23. Sonker, A. K., Rathore, K., Nagarale, R. K., & Verma, V. (2018). Crosslinking of polyvinyl alcohol (PVA) and effect of crosslinker shape (aliphatic and aromatic) thereof. *Journal of Polymers and the Environment, 26*, 1782–1794.
24. Strokov, K., Schäfer, A. H., Dobrindt, U., & Galstyan, A. (2020). Facile fabrication of silicon(iv)phthalocyanine-embedded poly(vinyl alcohol)-based antibacterial and antifouling interfaces. *ACS Applied Bio Materials, 3*, 3751–3760.
25. Martin-Martinez, F. J., Jin, K., López Barreiro, D., & Buehler, M. J. (2018). The rise of hierarchical nanostructured materials from renewable sources: learning from nature. *ACS Nano, 12*, 7425–7433.
26. Wang, T., Ke, H., Chen, S., Wang, J., Yang, W., Cao, X., Liu, J., Wei, Q., Ghiladi, R. A., & Wang, Q. (2021). Porous protoporphyrin IX-embedded cellulose diacetate electrospun microfibers in antimicrobial photodynamic inactivation. *Materials Science and Engineering: C, 118*, 111502.
27. Laroche, C., Delattre, C., Mati-Baouche, N., Salah, R., Ursu, V. A., Moulti-Mati, F., Michaud, P., & Pierre, G. (2018). Bioactivity of chitosan and its derivatives. *Current Organic Chemistry, 22*, 641–667.
28. Kalantari, K., Afifi, A. M., Jahangirian, H., & Webster, T. J. (2019). Biomedical applications of chitosan electrospun nanofibers as a green polymer—Review. *Carbohydrate Polymers, 207*, 588–600.
29. Sargazi, G., Afzali, D., Mostafavi, A., Shadman, A., Rezaee, B., Zarrintaj, P., Saeb, M. R., Ramakrishna, S., & Mozafari, M. (2019). Chitosan/polyvinyl alcohol nanofibrous membranes: Towards green super-adsorbents for toxic gases. *Heliyon, 5*, e01527.
30. Karim, M. R., Aijaz, M. O., Alharth, N. H., Alharbi, H. F., Al-Mubaddel, F. S., & Awual, M. R. (2019). Composite nanofibers membranes of poly(vinyl alcohol)/chitosan for selective lead(II) and cadmium(II) ions removal from wastewater. *Ecotoxicology and Environmental Safety, 169*, 479–486.
31. Wang, S., Yan, F., Ren, P., Li, Y., Wu, Q., Fang, X., Chen, F., & Wang, C. (2020). Incorporation of metal-organic frameworks into electrospun chitosan/poly(vinyl alcohol) nanofibrous membrane with enhanced antibacterial activity for wound dressing application. *International Journal of Biological Macromolecules, 158*, 9–17.
32. Fathollahipour, S., Abouei Mehrizi, A., Ghaee, A., & Koosha, M. (2015). Electrospinning of PVA/chitosan nanocomposite nanofibers containing gelatin nanoparticles as a dual drug delivery system. *Journal of Biomedical Materials Research Part A, 103*, 3852–3862.
33. Qiu, H., Zhu, S., Pang, L., Ma, J., Liu, Y., Du, L., Wu, Y., & Jin, Y. (2020). ICG-loaded photodynamic chitosan/polyvinyl alcohol composite nanofibers: Anti-resistant bacterial effect and improved healing of infected wounds. *International Journal of Pharmaceutics, 588*, 119797.
34. Strokov, K., & Galstyan, A. (2020). Chitosan–silicon phthalocyanine conjugate as effective photo-functional hydrogel for tracking and killing of bacteria. *European Journal of Organic Chemistry, 2020*, 7327–7332.
35. Huang, Z.-M., Zhang, Y. Z., Kotaki, M., & Ramakrishna, S. (2003). A review on polymer nanofibers by electrospinning and their applications in nanocomposites. *Composites Science and Technology, 63*, 2223–2253.
36. Supaphol, P., & Chuangchote, S. (2008). On the electrospinning of poly(vinyl alcohol) nanofiber mats: A revisit. *Journal of Applied Polymer Science, 108*, 969–978.
37. Karimi, M. A., Pourhakkak, P., Adabi, M., Firoozi, S., Adabi, M., & Naghibzadeh, M. (2015). Using an artificial neural network for the evaluation of the parameters controlling PVA/chitosan electrospun nanofibers diameter. *Polymers, 15*, 127–138.

38. Su, H., Fujiwara, T., & Bumgardner, J. D. (2021). A study of combining elastin in the chitosan electrospinning to increase the mechanical strength and bioactivity. *Marine Drugs, 19*, 169.
39. Su, H., Liu, K.-Y., Karydis, A., Abebe, D. G., Wu, C., Anderson, K. M., Ghadri, N., Adatrow, P., Fujiwara, T., & Bumgardner, J. D. (2016). In vitro and in vivo evaluations of a novel post-electrospinning treatment to improve the fibrous structure of chitosan membranes for guided bone regeneration. *Biomedical Materials, 12*, 015003.
40. Su, L., Huang, J., Li, H., Pan, Y., Zhu, B., Zhao, Y., & Liu, H. (2021). Chitosan-riboflavin composite film based on photodynamic inactivation technology for antibacterial food packaging. *International Journal of Biological Macromolecules, 172*, 231–240.
41. Tsai, T., Chien, H. F., Wang, T. H., Huang, C. T., Ker, Y. B., & Chen, C. T. (2011). Chitosan augments photodynamic inactivation of gram-positive and gram-negative bacteria. *Antimicrobial Agents and Chemotherapy, 55*, 1883–1890.
42. Zhang, R., Li, Y., Zhou, M., Wang, C., Feng, P., Miao, W., & Huang, H. (2019). Photodynamic chitosan nano-assembly as a potent alternative candidate for combating antibiotic-resistant bacteria. *ACS Applied Materials and Interfaces, 11*, 26711–26721.
43. Ke, C.-L., Deng, F.-S., Chuang, C.-Y., & Lin, C.-H. (2021). Antimicrobial actions and applications of chitosan. *Polymers, 13*, 904.
44. Maldonado-Carmona, N., Ouk, T.-S., & Leroy-Lhez, S. (2021). Latest trends on photodynamic disinfection of Gram-negative bacteria: photosensitizer's structure and delivery systems. *Photochemical and Photobiological Sciences, 21*, 113–145.
45. Galstyan, A., Majiya, H., & Dobrindt, U. (2022). Regulation of photo triggered cytotoxicity in electrospun nanomaterials: Role of photosensitizer binding mode and polymer identity. *Nanoscale Advances, 4*, 200–210.
46. Ghareeb, C. R., Peddinti, B. S. T., Kisthardt, S. C., Scholle, F., Spontak, R. J. & Ghiladi, R. A. (2021) Toward universal photodynamic coatings for infection control. *Frontiers in Medicine, 8,* 657837.
47. Song, F., Koo, H., & Ren, D. (2015). Effects of material properties on bacterial adhesion and biofilm formation. *Journal of Dental Research, 94*, 1027–1034.
48. Mosinger, J., Lang, K., Hostomský, J., Franc, J., Sýkora, J., Hof, M., & Kubát, P. (2010). Singlet oxygen imaging in polymeric nanofibers by delayed fluorescence. *The Journal of Physical Chemistry B, 114*, 15773–15779.
49. Skovsen, E., Snyder, J. W., Lambert, J. D. C., & Ogilby, P. R. (2005). Lifetime and diffusion of singlet oxygen in a cell. *The Journal of Physical Chemistry B, 109*, 8570–8573.
50. Imlay, J. A. (2003). Pathways of oxidative damage. *Annual Review of Microbiology, 57*, 395–418.
51. Di Novo, N. G., Carotenuto, A. R., Mensitieri, G., Fraldi, M. & Pugno, N. M. (2021) Modeling of virus survival time in respiratory droplets on surfaces: A new rational approach for antivirus strategies. *Frontiers in Materials, 8,* 631723.
52. Si, Y., Zhang, Z., Wu, W., Fu, Q., Huang, K., Nitin, N., Ding, B., & Sun, G. (2018). Daylight-driven rechargeable antibacterial and antiviral nanofibrous membranes for bioprotective applications. *Science Advances, 4*, eaar5931.
53. Käsermann, F., & Kempf, C. (1997). Photodynamic inactivation of enveloped viruses by buckminsterfullerene1For the described inactivation procedure, a patent application was submitted.1. *Antiviral Research, 34*, 65–70.
54. Costa, L., Faustino, M. A. F., Neves, M. G. P. M. S., Cunha, Â., & Almeida, A. (2012). Photodynamic inactivation of mammalian viruses and bacteriophages. *Viruses, 4*, 1034–1074.
55. Wiehe, A., O'Brien, J. M., & Senge, M. O. (2019). Trends and targets in antiviral phototherapy. *Photochemical and Photobiological Sciences, 18*, 2565–2612.
56. Abe, H., & Wagner, S. J. (1995). Analysis of viral DNA, protein and envelope damage after methylene blue, phthalocyanine derivative or merocyanine 540 photosensitization. *Photochemistry and Photobiology, 61*, 402–409.

Authors and Affiliations

Anzhela Galstyan[1,2] · Konstantin Strokov[2]

[1] Faculty of Chemistry, Center for Nanointegration Duisburg-Essen (CENIDE) and Centre for Water and Environmental Research (ZWU), University of Duisburg-Essen, Essen, Germany

[2] Center for Soft Nanoscience, University of Münster, Münster, Germany